Spatiotemporal characterization of summer coastal upwelling events in Uruguay, South America

Romina Trinchin [a,*], Leonardo Ortega [b], Marcelo Barreiro [a]

[a] *Department of Atmospheric Sciences, Institute of Physics, Universidad de la República, Iguá 4225, Montevideo 11400, Uruguay*
[b] *National Direction of Aquatic Resources, Constituyente 1497, Montevideo 11200, Uruguay*

ARTICLE INFO

ABSTRACT

This study analyses the spatial and temporal characteristics of coastal upwelling events in the Uruguayan coast using satellite data and the output of an atmospheric reanalysis. We focus on the most intense upwelling events which occurred on synoptic time scales during the summer season. We were able to distinguish two upwelling configurations associated to different wind conditions due to the coast orientation: an upwelling mainly located in the Río de la Plata estuary which responds to easterly winds, and an oceanic upwelling located in the eastern (oceanic) coast of Uruguay associated to northeasterly winds. Moreover, the frequency of occurrence of upwelling events on interannual time scales was found to depend on the phase of El Niño Southern Oscillation.

© 2019 Elsevier B.V. All rights reserved.

1. Introduction

Coastal upwelling events have been reported in the Uruguayan coast as frequent and persistent and also seasonally variable (Simionato et al., 2010). The first study describing the occurrence of these events is the one by Framiñan et al. (1999), which used daily satellite data of sea surface temperature (SST) of 1.1 km horizontal resolution. They identified the upwelling as a cooling along the coast with values 4 and 5 °C colder than the surrounding waters, located between Punta del Este and Cabo Polonio (Fig. 1). Moreover, they found its occurrence under synoptic N-NE direction winds and a minimum discharge of the Río de la Plata estuary. Pimenta et al. (2008) registered two upwelling events with in situ data at the same location and under the same conditions as described by Framiñan et al. (1999). Subsequently, Simionato et al. (2010) analysed SST variability in the Río de la Plata estuary on seasonal and sub-annual time scales using daily satellite images of 11 km of horizontal resolution for the period 2002–2008. They found evidence of upwelling events under northeasterly winds and defined them as frequent and seasonally variable. More recent studies using a hydrodynamic model of the Río de la Plata (Meccia et al., 2013) found the occurrence of upwelling events in a similar location as the one reported by Simionato et al. (2010). Finally, works using altimetry data show a minimum of sea level height in the Uruguayan coast during summer, in agreement with Ekman transport due to the prevalent winds that blow parallel to the coast in this season (Saraceno

et al., 2014; Strub et al., 2015). Thus, even though upwelling events in the Uruguayan coast have been reported and studied, there has been no recent systematic study of their spatial and temporal characteristics. The present study addresses these issues analysing satellite data and an atmospheric reanalysis considering a time series larger than previous works.

We considered the area defined by 30–38°S and 50–59°W, which includes the Uruguayan coast (Fig. 1). This area is characterized by a marked spatio-temporal variability and high productivity (Guerrero and Piola, 1997; Acha et al., 2008; Martínez and Ortega, 2015). It is part of a complex hydrological system that comprises the frontal zone of the Río de la Plata estuary (RdlP) and the Atlantic Ocean. This is a transitional zone influenced by waters with contrasting features: warm and saline tropical waters from a branch of the Brazil Current and cold diluted Subantarctic waters derived from the Malvinas Current (Guerrero et al., 1997). The RdlP estuary flows through the Atlantic Ocean with an average discharge of 22,000 m^3/s, that has low seasonality and large interannual variability (Piola et al., 2005). Moreover, this area is very sensitive to atmospheric forcing (Guerrero et al., 1997; Simionato et al., 2004; Meccia et al., 2013), and the circulation is dominated by the wind stress (Simionato et al., 2008). Winds change direction with the season, being predominantly from S-SW during winter and from N-NE during summer (Simionato et al., 2005).

2. Data

Sea surface temperature measurements from daily satellite data L3-mapped images of 4 km horizontal resolution from the

---

* Corresponding author.
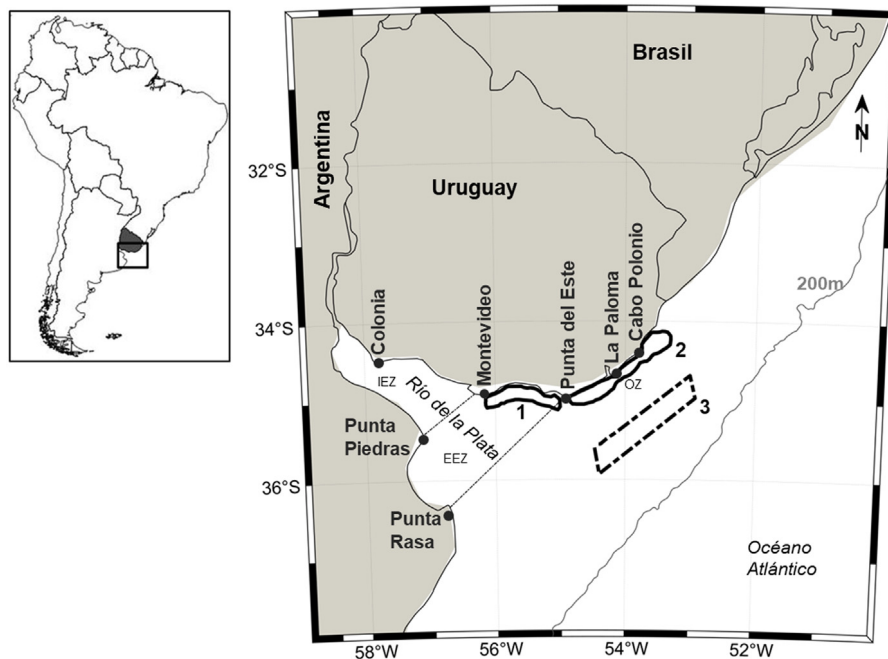*E-mail address:* rtrinchin@fisica.edu.uy (R. Trinchin).

Fig. 1. Study area showing the geographical location where coastal upwelling processes occur. The figure illustrates three zones within the Rio de la Plata estuary: Intermediate estuary zone (IEZ), external estuary zone (EEZ) and oceanic zone (OZ). Also shown are the 200 m isobath and coastal locations. Three irregular polygons are referenced with numbers for the analysis in Section 4: (1) is the area of influence of estuarine upwelling; (2) the corresponding for oceanic upwelling and (3) is an offshore external box.

sensor MODIS-Aqua were used (freely available at https://oceancolor.gsfc.nasa.gov/). Atmospheric variables including sea level pressure and surface winds (10 m) from the European Centre for Medium-Range Weather Forecasts Interim Reanalysis (ERA-Interim) were used to characterize the synoptic configuration related to upwelling conditions. The ERA-Interim reanalysis product (Dee et al., 2011) has a daily temporal resolution and horizontal spatial resolution of 0.125° x 0.125°. For oceanic and atmospheric variables the period analysed spanned from 1 January 2003 to 31 December 2014, considering only the summer season (December, January and February, hereafter DJF) when wind direction favours coastal upwelling (Framiñan et al., 1999; Simionato et al., 2005) and according to Simionato et al. (2010) upwelling events are more frequent (∼60%). Finally, we considered the Rio de la Plata discharge provided by Instituto Nacional del Agua Argentina (Borús, 2019). Daily anomalies of each variable were calculated as the difference between the observed value and the daily climatology for the period 2003–2014. The SST was smoothed with a 2-day moving average because of missing data.

3. Characterization of upwelling events

3.1. Climatology

Summer season and monthly climatologies for the study area show a temperature gradient with warmer temperatures to the north, and colder temperatures to the south (Fig. 2), as expected (e.g. Guerrero et al., 1997). A thermal gradient can be appreciated from the inner to the outer part of the RdlP estuary. Moreover, in particular during December and February on the southeastern Uruguayan coast there is an area centred at La Paloma (∼−34.7°S, 54.1°W) that is relatively colder than the surrounding area, which may be associated with the upwelling associated with the mean climatological winds. In this study we focus on deviations from this climatology, and thus we are concerned with the high frequency upwelling events generated by high frequency atmospheric transients.

3.2. Spatial structure of upwelling events

In order to explore the variability of sea surface temperature anomalies (SSTa, see Section 2) Empirical Orthogonal Functions (EOFs) were calculated for the domain within 33.5°S–35.5°S and 53.5°W–56.5°W. The area was chosen to focus on the processes that occur along the Uruguayan coast and to minimize calculation problems with missing data. The first three principal components (PCs) explain 78% of the variance. The first EOF (EOF1) represents 58% of the total variance and it has the same sign in the entire region, probably related to heat flux exchanges between the ocean and the atmosphere (not shown). The EOF2 and EOF3 have maximum SSTa next to the coast, as expected for coastal upwelling (Fig. 3), and will be considered here as representing this phenomenon keeping in mind that only the positive phases of PC2 and PC3 do it (see below). EOF2 presents an upwelling area that has maximum anomalies from Montevideo to Punta del Este located in the estuarine coast (See Fig. 1). EOF3 shows another upwelling configuration located in the Atlantic coast between Punta del Este and Cabo Polonio. Considering the locations, EOF2 will be named as estuarine upwelling and EOF3 as oceanic upwelling events. It is important to note that EOF2 has also areas of significant anomalies on the oceanic region, and thus there will be cases in which estuarine and oceanic regions behave in the same way. From the EOF maps we estimate the area occupied by the events considering the isoline of −0.2 °C. The area was approximated as that defined by a rectangle given by the distance along the coastline between the ends of the isoline of −0.2 °C, and the maximum distance between the coast and the -0.2 °C isoline. As a result we estimated an area of 19,500 km^2 and 8500 km^2 for the estuarine and oceanic upwelling, respectively. The estimation for the estuarine upwelling agrees with previous work (∼20,000 km^2, Simionato et al., 2010). These results represent mean upwelling conditions.

Considering the EOFs that represent upwelling events, composites for positive (>1 standard deviation) and negative (<1 standard deviation) phases of each PC for the variables SSTa, SST,
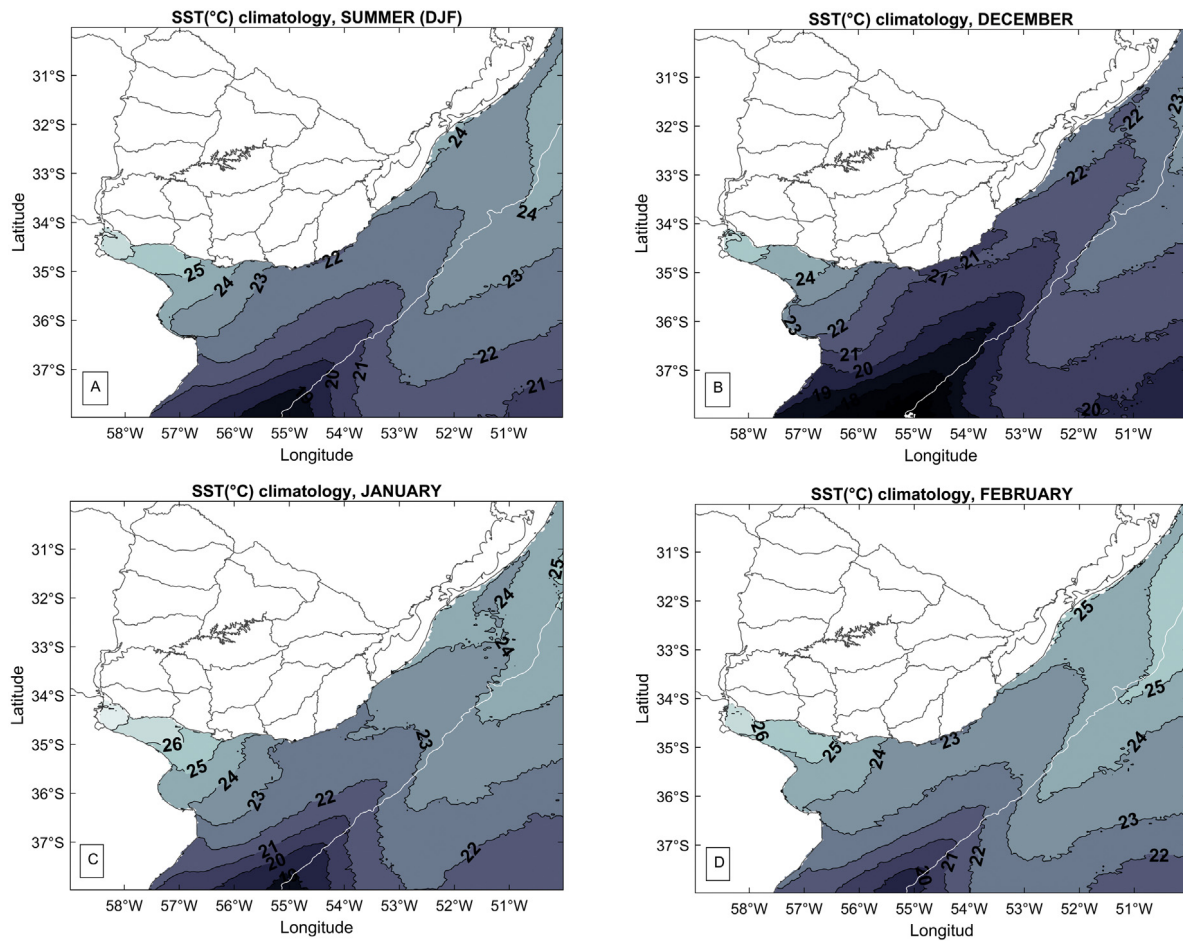
Fig. 2. (a) Summer (DJF) and (b, c, d) monthly climatology of sea surface temperature (°C); the white line is the 200 m isobath and the numbers in contour are sea surface temperature (°C) values.
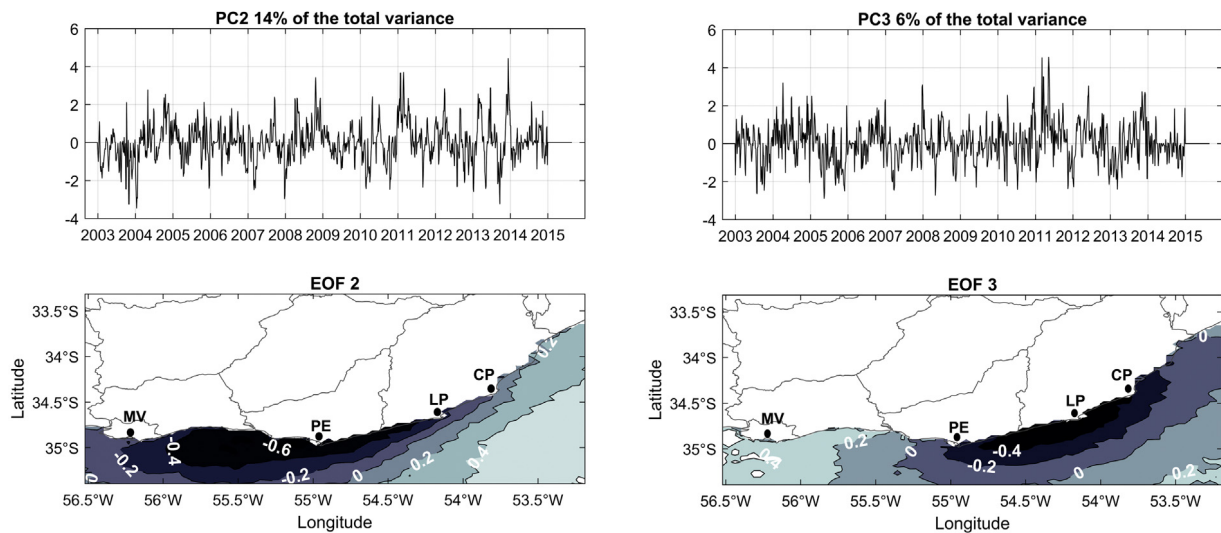

Fig. 3. Modes of variability of sea surface temperature anomaly in the domain considered. Empirical orthogonal function (EOFs) and Principal component time series (PCs) which represents 14% and 6% of the total variance. Coastal localities are indicated with black dots: Montevideo (MV), Punta del Este (PE), La Paloma (LP) and Cabo Polonio (CP)

wind anomaly and wind were constructed (see Figs. 4 and 5). As mentioned before, positive phases of PC2 and PC3 represent up-welling and favourable wind conditions while the negative phases represent non-favourable upwelling conditions. From composite analysis we estimated intense SSTa and SST values.

Estuarine upwelling (PC2, Fig. 4 upper panels) has values of SSTa ranging from −2 to −0.5 °C. In the upwelling region SST ranged from 20 to 22 °C which is between 4 and 1 °C colder than surrounding offshore waters. The spatial structure of the anomalous composite is similar to the composite of the negative
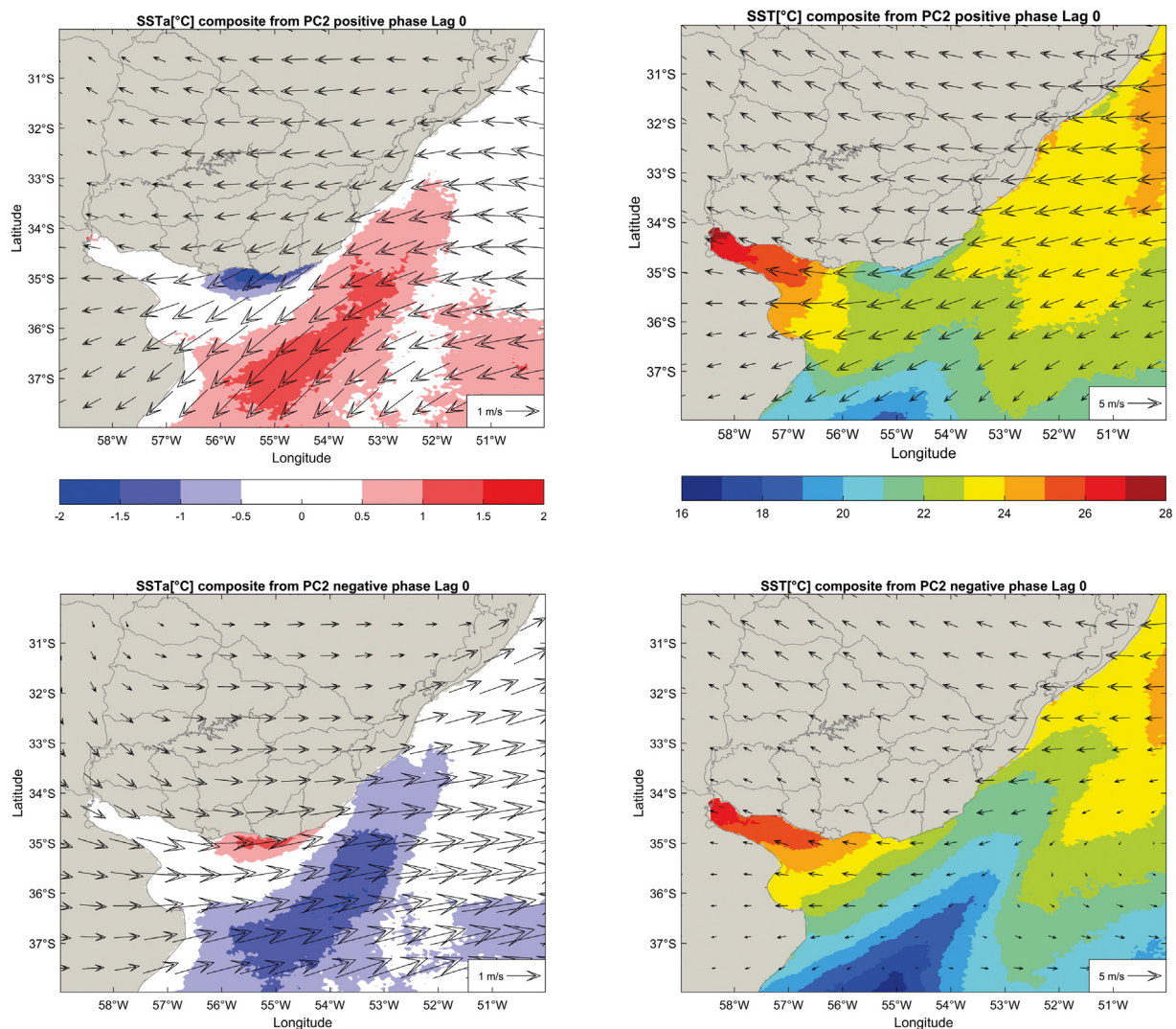
Fig. 4. Composites of sea surface temperature and wind anomalies (left) and sea surface temperature and wind (right) for positive (upper) and negative (lower) phases of PC2. Figures at the top represent estuarine upwelling.

phase of the first mode of sub-annual SSTa variability analysed by Simionato et al. (2010). On the other hand, the negative phase (Fig. 4 lower panels) represents non-favourable upwelling conditions showing positive SSTa between 0.5 and 1.5 °C in the coast that can be seen as an accumulation of RdlP waters on Uruguayan shoreline. Also wind anomalies are from the west, which weaken the northeasterlies and are not upwelling favourable. The SST map suggests the intrusion of Malvinas current on the continental shelf.

Composites for PC3 shows oceanic upwelling in the positive phase (Fig. 5 upper panels). This upwelling type has negative SSTa values between −0.5 and −1.5 °C and SST in the upwelling area ranged between 20–22 °C similar as for the estuarine upwelling. In this case SST is 1 °C colder than surrounding offshore waters. In contrast PC3 composites in the negative phase show a warming in the oceanic upwelling area with an SSTa between 0.5 – 1.5 °C and a cooling in the inner estuary (Fig. 5 lower panels). Those anomalies are consistent with an intrusion of the RdlP waters toward the Uruguayan Atlantic coast forced by southwesterly winds. As result the estuary shows relatively uniform SSTs.

In Figs. 4 and 5 it is possible to see that each upwelling type (estuarine or oceanic) is associated with a different wind configuration following the changes in the orientation of the coast. Particularly, for estuarine upwelling the wind anomalies

(1 m/s) blow predominantly from the east, reinforcing the mean winds parallel to the coast with maximum intensities of 6 m/s (Fig. 4). In the case of oceanic upwelling the wind anomalies are characterized by winds from the northern sector accompanying the change in the coastal orientation with maximum intensities of 5 m/s and anomalies of 1 m/s from the same direction.

3.3. Evolution of upwelling events

In this subsection we use Pearson correlation and regression analyses to determine the joint atmosphere-ocean evolution during estuarine and oceanic events. Statistical significance is computed using a two-sided T-test at 5% significance level. The correlation of PC2 and PC3 with SSTa shows dipole structures principally at lag 0 (Figs. 6 and 7). In the estuarine coast there is a dipole between the maximum negative correlation in the area of upwelling and a maximum positive correlation area far from the coast to the east (Fig. 6). In the oceanic case, the dipole is between a maximum negative correlation in the area of upwelling and a maximum positive correlation in RdlP (Fig. 7). Both correlation maps are consistent with the composites. Also, the estuarine events persist longer than the oceanic events which spatial extent is mainly evident during day 0 (Figs. 6 and 7). In both types of upwelling maximum wind anomalies develop during day -1
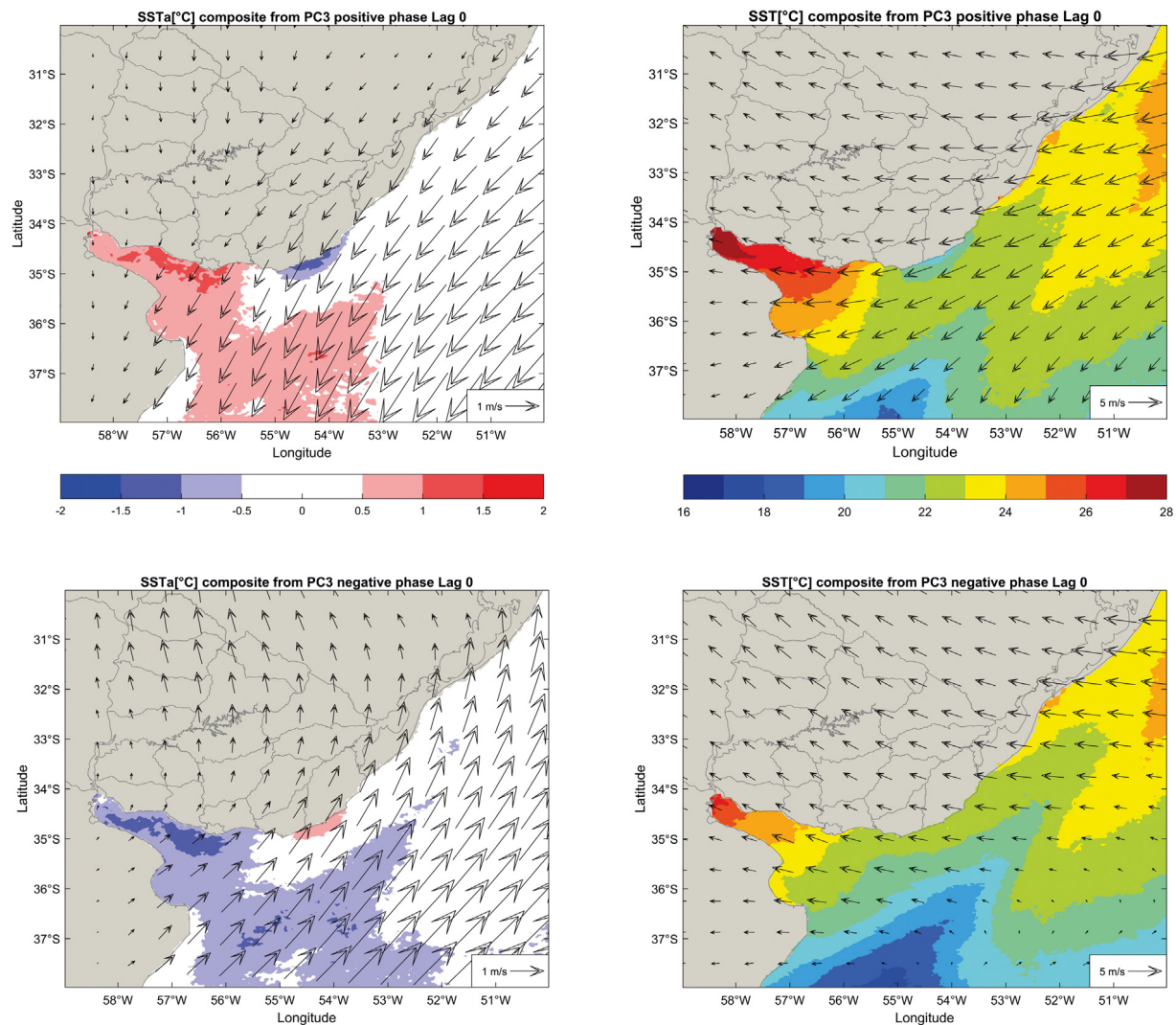
Fig. 5. Composites of sea surface temperature and wind anomalies (left) and sea surface temperature and wind (right) for positive (upper) and negative (lower) phases of PC3. Figures at the top represent oceanic upwelling.

and persist until day 0. This suggests a delay of 1 day in the ocean's response to the atmospheric forcing and, in the estuarine case that once the cold water has upwelled it can persist after the forcing disappears. The estuarine case is characterized by a high (low) pressure system to the southeast (northwest) of Uruguay consistent with the wind anomalies. On the other hand the oceanic events present a strong zonal pressure gradient that develops due to a low pressure centre located to the west and a high pressure centre to the east over the Atlantic Ocean. In both cases upwelling favourable conditions end with the displacement of the low pressure centres to the east.

4. Classification of intense upwelling events with a coastal index and interannual variability

The EOF2 and EOF3 are orthogonal by construction and have maximum weight in different coastal regions. Nonetheless, EOF2 has also weight east of Punta del Este, the region that characterizes EOF3. To complement that analysis we built two coastal indexes by averaging SSTa in the two separated coastal regions marked in Fig. 1. Moreover, we focus on intense upwelling events and their dependence on river discharge and ENSO occurrence.

The coastal boxes identified as 1 (2) in Fig. 1 is named CE (CO) for the region of the coast where estuarine (oceanic) upwelling

has largest influence. Moreover, we considered a box named E far from the coast where upwelling dynamics is not important (marked as 3 in Fig. 1). To identify intense upwelling events we applied three conditions that must be fulfilled simultaneously: (1) consecutive days with negative SSTa with at least one day with anomalies equal or under −0.5 °C in coastal boxes; (2) discard days with more than 50% with missing data in coastal boxes; (3) negative SSTa in coastal boxes must be at least −1.5 °C less than the SSTa in the external box. As result a total of 33 intense events were identified for summer in the period considered (2003–2014), 12 of these corresponding to estuary upwelling and 21 to oceanic upwelling with durations that vary between 1 and 4 days (Fig. 8). Note that in this analysis oceanic upwelling events may last up to 4 days, more than the events derived from the EOF analysis, and local anomalies of up to −4 °C (not shown) consistent with literature (Simionato et al., 2010). This suggests that intense upwelling events last more than weaker ones on average.

We next explore the relationship between RdlP discharge and the occurrence of both upwelling types (Fig. 9). We found that of the 33 days with oceanic upwelling, 70% of them occurred under negative discharge anomaly conditions and 21% occurred between 0 and +1 standard deviation, and 9% were observed above +1 standard deviation. In the case of estuarine upwelling
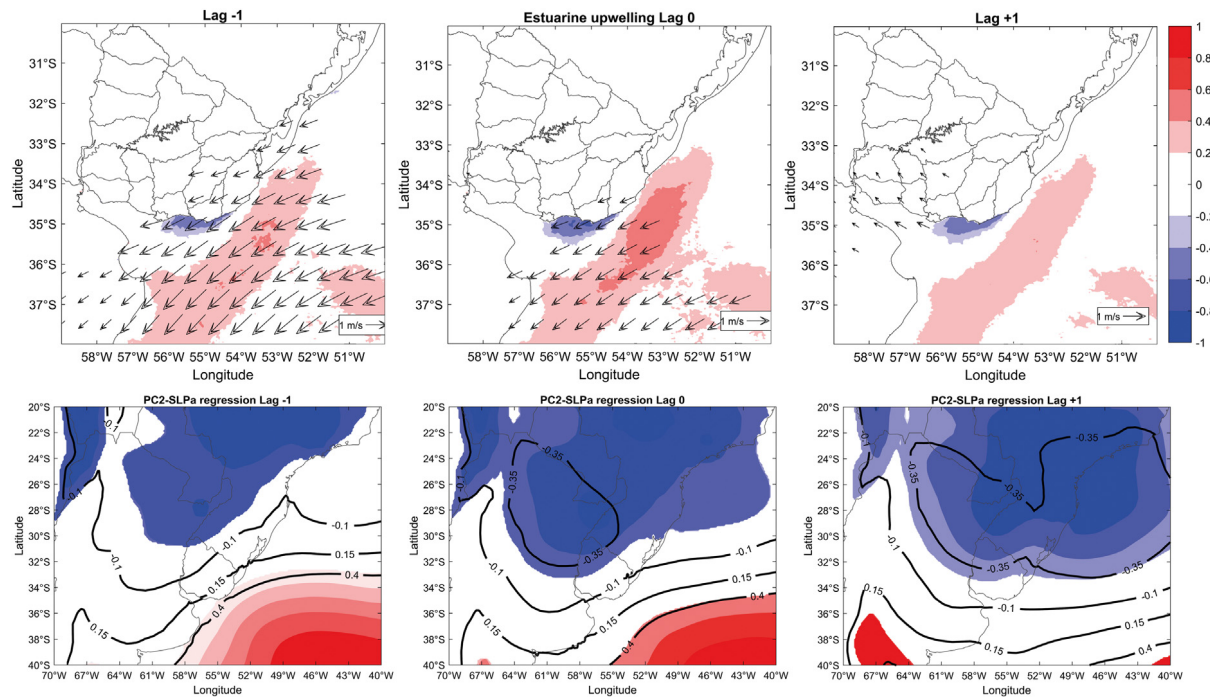
Fig. 6. Correlation coefficient of PC2 with sea surface temperature anomaly and surface winds (upper row). Colour scale indicates the value of the correlation coefficients of SSTa at intervals of 0.2, with white areas indicating correlation values not different from 0. The lower row shows regression maps for pressure anomalies in contours (0.25 intervals) and its statistical significance in colours measured by the T-test.
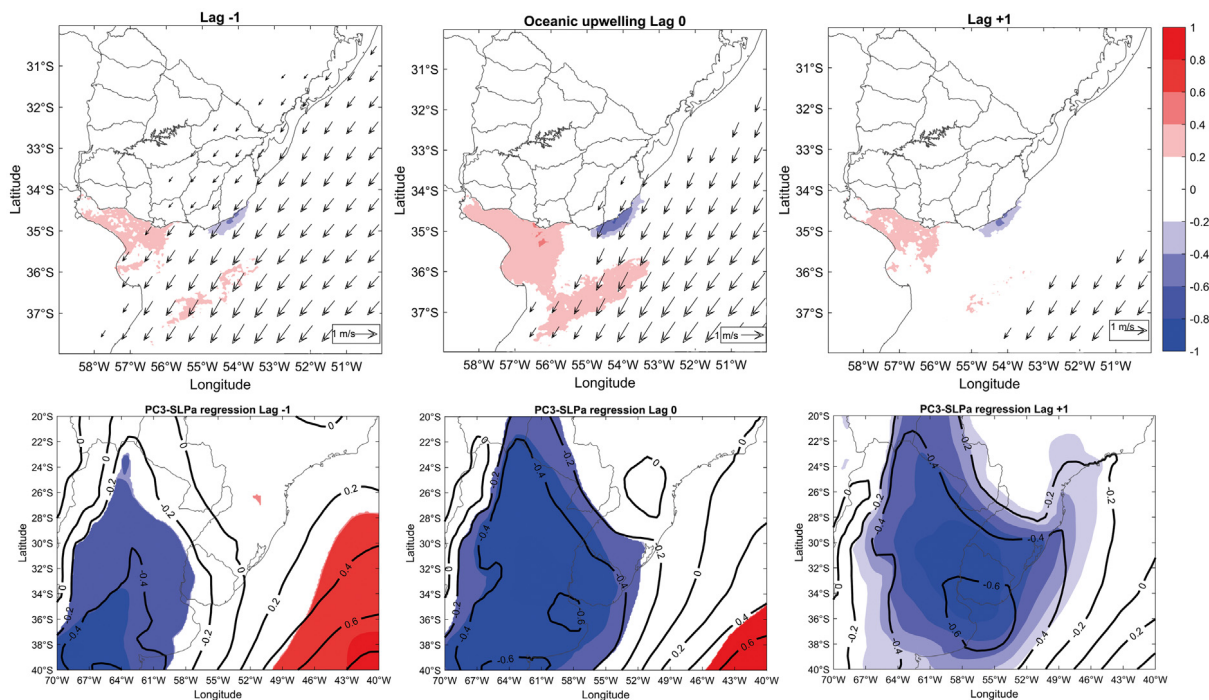

Fig. 7. Analogous to Fig. 6, but for PC3.

from a total of 17 days, 76.5% occurred under negative discharge conditions, 11.75% occurred between 0 and +1 standard deviation, and 11.75% were above +1 standard deviation. Hence most of the upwelling events occurred under low discharge conditions, in agreement with previous results using shorter data sets (Pimenta et al., 2008; Simionato et al., 2010).

The days that occurred during the positive anomaly peak of the discharge correspond to dates 28/12/2010 and 30-31/12/2010.

During these particular events satellite images reveal that warm waters associated with the RdlP discharge are located over the southern part of the estuary mainly in Samborombon Bay (not shown), and thus may not have influenced the occurrence of upwelling in the Uruguayan coast. More research is needed to further understand these events considering the relationship between the path of the Rio de la Plata plume and the discharge of its main tributaries (Simionato et al., 2009; Silva et al., 2014).
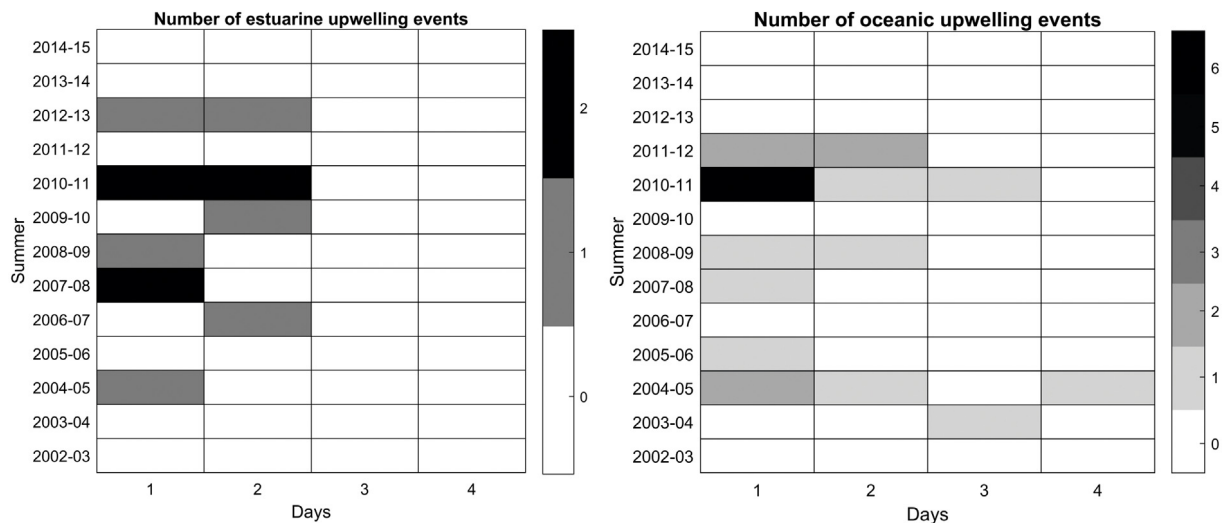
Fig. 8. Upwelling events identified in region CE (left) and region CO (right). The figure represents the number of events identified in each summer period separated by time duration. *x* axis represents time duration in days, *y* axis is the summer period in years and the colour bar is the number of events.
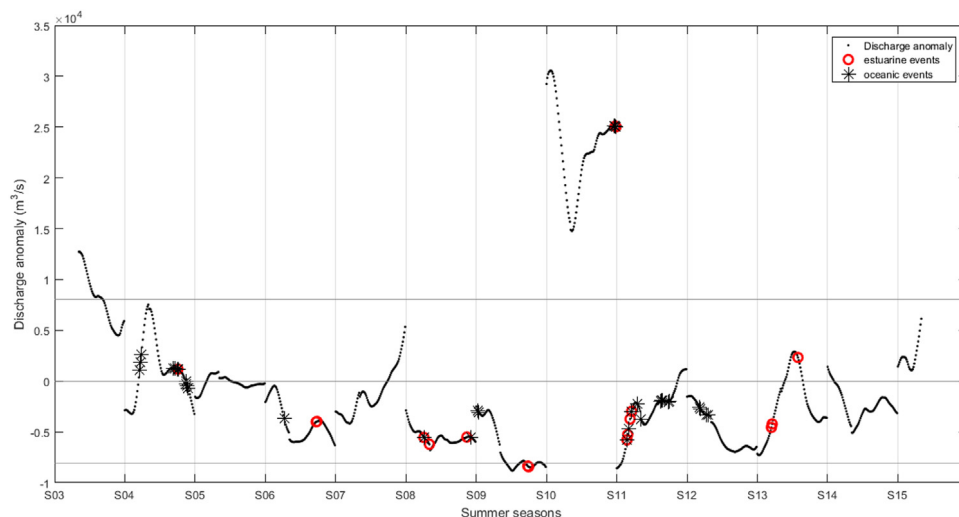

Fig. 9. Rio de la Plata daily discharge anomaly for summer seasons (December–January–February) from summer 2002–2003 (S03) to summer 2014–2015 (S15). Red points are intense oceanic upwelling events and black asterisks are intense estuarine upwelling events. Grey lines show one standard deviation.

The relationship between ENSO and the occurrence of upwelling events was also analysed. To do so we counted the total number of upwelling events (estuarine plus oceanic) that occurred in El Niño, La Niña and neutral years (Fig. 10). Statistical differences between ENSO phases were compared using the Kruskal–Wallis non-parametric test (Zar, 1999) at 10% significance level. Results show that more upwelling events occurred during La Niña years compared to during El Niño years and are statistically significant at the 10% level. Although statistics are not very robust due to the shortness of the time series it is possible to find plausible physical arguments to support this result following the studies of Pimenta et al. (2008) and Simionato et al. (2010). Under La Niña conditions spring and summer rainfall over southeastern South America decreases (Barreiro, 2010), leading to a reduction in the discharge of the RdlP. Consequently, the water column becomes less stable being easier for the wind to break-up that stability and therefore generate upwelling. Thus, it would be expected to find more upwelling events during la Niña. Moreover, in La Niña years anomalous easterly winds parallel to the coast are generated in this region (Piola et al., 2005; Barreiro, 2017).

5. Discussion and conclusions

The results of this work are a contribution to the understanding of the upwelling processes that occur in the Uruguayan coast. In particular this study analyses a longer and higher resolution data set (12 year) than considered in previous studies. This allowed distinguishing between two different upwelling structures which respond to different atmospheric circulation configurations and named in this work as Estuarine and Oceanic upwelling.

Given that previous studies had only documented one type of upwelling event we performed a sensitivity test to address the effect of spatial resolution. To do so we repeated the EOF analysis after filtering the data as in Simionato et al. (2010). That is, we removed the interannual variability and smoothed the data with a 5-day moving average. Moreover, the grid resolution was reduced to ∼12 km, and the domain increased to [33–37°S, 51.9–56.5°W]. The resulting EOF2 and EOF3 are shown in Fig. 11. The EOF analysis recovers the estuarine upwelling structure in EOF2 associated with the same atmospheric configuration as found in Section 3. On the other hand, EOF3 does not show the oceanic upwelling (Fig. 11), even though characterized by a very similar atmospheric
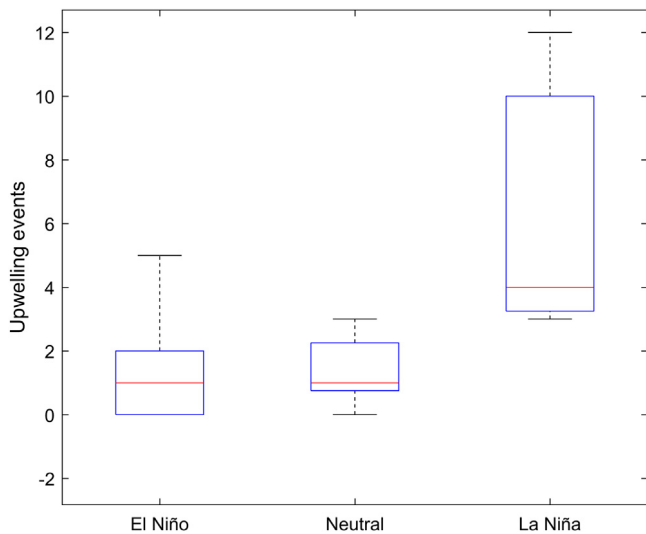
Fig. 10. Boxplot of upwelling events for each El Niño Southern Oscillation phase. Red lines represents median, box limits are percentile 75 and 25 (upper and lower respectively) and the whiskers area maximum and minimum values. This analysis considers oceanic and estuarine events together.

configuration to the one favourable for oceanic upwelling (compare with Fig. 7). This suggests that the 4 km spatial resolution

MODIS Aqua satellite data is suitable to resolve mesoscale coastal oceanographic process. This is particularly relevant for places, like Uruguay, where in situ data is scarce or difficult to access. It is worth mentioning that the first upwelling record in the literature (Framiñan et al., 1999; Pimenta et al., 2008) refer to oceanic upwelling events which come from very high spatial resolution satellite data (1.1 km) and in situ data, whereas more recent studies (Simionato et al., 2010; Meccia et al., 2013) are estuarine upwelling events. The latter confirmed previous results but did not discuss the different locations of the events.

We found that winds parallel to the coast are responsible of the generation of the upwelling events responding to a classical mechanism of upwelling generation proposed by Ekman (1905) even though the condition of infinite depth is not satisfied due to the shallowness of the system (<50 m). Thus, we reinforce the evidence found in previous studies that northeasterly winds are responsible for generating upwelling events in the coast of Uruguay between Punta del Este and Cabo Polonio (Framiñan et al., 1999; Pimenta et al., 2008). In contrast, our results stress the importance of easterly winds in the generation of estuarine upwelling. The differences in wind direction are closely related to changes in the orientation of the coast. The occurrence of upwelling events was found to vary mainly on synoptic time scales, and individual events tend to last less than 4 days.

As in previous studies wind and river discharge are identified as the principal upwelling drivers in this area (Framiñan et al., 1999; Pimenta et al., 2008; Simionato et al., 2010). However, other factors such as topography and coastal geomorphology,
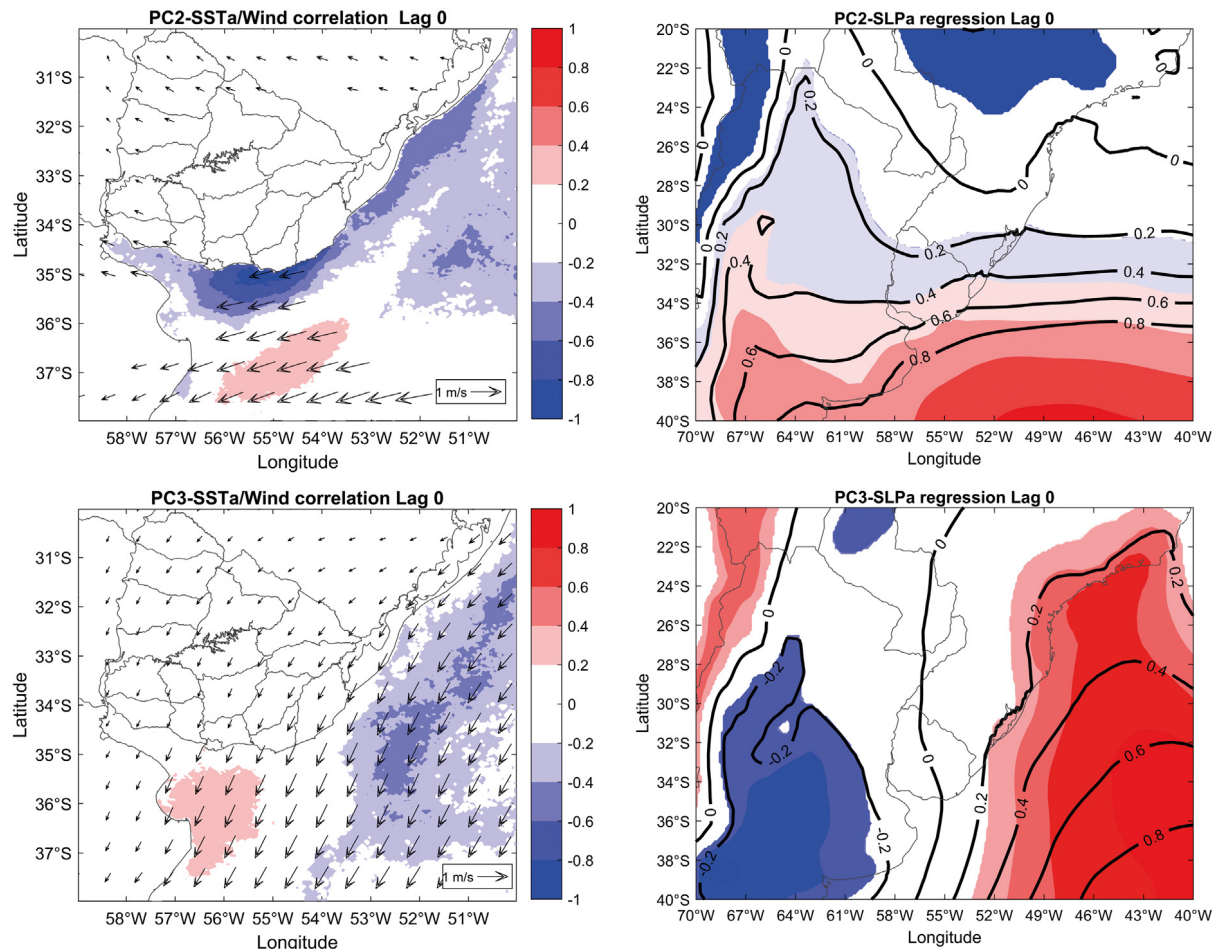

Fig. 11. Correlation of sea surface temperature anomaly and regression of sea level pressure and wind anomalies with the principal components (PC) derived from the sensitivity analysis. Upper is PC2 and lower is PC3 which represents 9.6% and 5% of the variance, respectively.

which were not considered thus far, also can influence upwelling processes. Therefore, it would be interesting to use a regional ocean model to test the sensitivity of upwelling to different bathymetries and coastal orientations.

Declaration of competing interest

The authors declare that they have no known competing financial interests or personal relationships that could have appeared to influence the work reported in this paper.

Acknowledgements and data

References

Acha, E.M., Mianzan, H., Guerrero, R.J.C., Giberto, D., Montoya, N., Carignan, M., 2008. An overview of physical and ecological processes in the Rio de la Plata Estuary. Cont. Shelf Res. 28, 1579–1588.

Barreiro, M., 2010. Influence of ENSO and the South Atlantic Ocean on climate predictability over Southeastern South America. Clim. Dynam. 35 (7–8), 1493–1508.

Barreiro, M., 2017. Interannual variability of extratropical transient wave activity and its influence on rainfall over Uruguay. Int. J. Climatol..

Borús, J., 2019. Evaluación de caudales diarios descargados por los grandes ríos del sistema del Plata al Río de la Plata. Dirección de Sistemas de Información y Alerta Hidrológico Instituto Nacional del Agua, Ezeiza, Argentina.

Dee, D.P., Uppalaa, S.M., Simmonsa, A.J., Berrisforda, P., Polia, P., Kobayashib, S., Andraec, U., Balmasedaa, M.A., Balsamoa, G., Bauera, P., Bechtolda, P., Beljaarsa, A.C.M., van de Bergd, L., Bidlota, J., Bormanna, N., Delsola, C., Dragania, R., Fuentesa, M., Geera, A.J., Haimbergere, L., Healya, S.B., Hersbacha, H., Holma, E.V., Isaksena, L., Kallbergc, P., Köhlera, M., Matricardia, M., McNallya, A.P., Monge-Sanzf, B.M., Morcrettea, J.J., Parkg, B.K., Peubeya, C., de Rosnaya, P., Tavolatoe, C., Thépauta, J.-N., Vitart, F., 2011. The ERA-interim reanalysis: configuration and performance of the data assimilation system. Q. J. R. Meteorol. Soc. 137, 553–597.

Ekman, V.W., 1905. On the influence of the earth's rotation on ocean currents. Ark. Mat. Atronomi Och Fysik 2 (11).

Framiñan, M.B., Etala, M.P., Acha, E.M., Guerrero, R.A., Lasta, C.A., Brown, O.B., 1999. Physical characteristics and processes of the Río de la Plata estuary. In Estuaries.

Guerrero, R.A., Acha, E.M., Framin, M.B., Lasta, C.A., 1997. Physical oceanography of the Río de la Plata Estuary, Argentina. Cont. Shelf Res. 17 (7), 727–742.

Guerrero, R.A., Piola, A.R., 1997. Water masses in the continental shelf. Argentine Sea Fish. Resour. 1, 107–118.

Martínez, A., Ortega, L., 2015. Delimitation of domains in the external Río de la Plata estuary, involving phytoplanktonic and hydrographic variables. Braz. J. Oceanogr. 63 (3), 217–227.

Meccia, V.L., Simionato, C.G., Guerrero, R.A., 2013. The Rio de la Plata Estuary response to wind variability in synoptic timescale: salinity fields and salt wedge structure. J. Coast. Res. 29 (1), 61–77.

Pimenta, F., Garvine, R.W., Münchow, A., 2008. Observations of coastal upwelling off Uruguay downshelf of the Plata estuary, South America. J. Mar. Res. 66 (6), 835–872.

Piola, A.R., Matano, R.P., Palma, E.D., Möller, O.O., Campos, E.J., 2005. The influence of the Plata River discharge on the western South Atlantic shelf. Geophys. Res. Lett. 32 (1).

Saraceno, M., Simionato, C.G., Ruiz-Etcheverry, L.A., 2014. Sea surface height trend and variability at seasonal and interannual time scales in the Southeastern South American continental shelf between 27 °s and 40 °s. Cont. Shelf Res. 91, 82–94.

Silva, C.P., Marti, C.L., Jörg, I., 2014. Horizontal transport, mixing and retention in a large, shallow estuary: Río de la Plata. Environ. Fluid Mech. 14 (2014), 1173–1197.

Simionato, C.G., Berasategui, A., Meccia, V.L., Acha, M., Mianzan, H., 2008. Short time-scale wind forced variability in the Río de la Plata Estuary and its role on ichthyoplankton retention. Estuar. Coast. Shelf Sci. 76 (2), 211–226.

Simionato, C.G., Dragani, W., Meccia, V., Nuñez, M., 2004. A numerical study of the barotropic circulation of the Ríó de la Plata estuary: sensitivity to bathymetry, the Earth's rotation and low frequency wind variability. Estuar. Coast. Shelf Sci. 61 (2), 261–273.

Simionato, C.G., Meccia, Dragani, W.C., 2009. On the path of plumes of the Rio de la Plata Estuary main tributaries and their mixing scales. Geoacta 34, 87–116.

Simionato, C.G., Tejedor, M.L.C., Campetella, C., Guerrero, R., Moreira, D., 2010. Patterns of sea surface temperature variability on seasonal to sub-annual scales at and offshore the Río de la Plata estuary. Cont. Shelf Res. 30 (19), 1983–1997.

Simionato, C.G., Vera, C., Siegismund, F., 2005. Surface wind variability on seasonal and interannual scales over Río de la Plata area. J. Coast. Res. 21, 770–783.

Strub, P.T., James, C., Combes, V., Matano, R.P., Piola, A.R., Palma, E.D., …, Ruiz-Etcheverry, L.A., 2015. Altimeter-derived seasonal circulation on the southwest atlantic shelf: 27°-43° s. J. Geophys. Res.: Oceans 120 (5), 3391–3418.

Zar, J.H., 1999. Biostatistical Analysis, fourth ed. Prentice Hall, New Jersey, p. 929.